The final publication is available at Earthquake Engng Struct Dyn. 2018;1–21. https://doi.org/10.1002/eqe.3115

Evolution of Out-of-plane Deformation and Subsequent Instability in Rectangular RC Walls under In-plane Cyclic Loading; Experimental Observation

Farhad Dashti[1]; Rajesh P Dhakal[2]; and Stefano Pampanin[3]

ABSTRACT

In this study, in order to understand the causes and consequences of out-of-plane instability in rectangular RC walls, the sequence of events observed during a rectangular wall experiment campaign where out-of-plane instability was the primary failure pattern is discussed in detail. Large tensile strains developed in the boundary zone longitudinal bars at large in-plane curvature demands and caused subsequent yielding in compression during load reversal before crack closure could activate contribution of concrete to the load-carrying capacity of the wall. The specimen deformed in the out-of-plane direction when this phenomenon progressed along a sufficient height and length of the wall and led to significant reduction of its stiffness in the out-of-plane direction. One of the major sources of inherent eccentricity that could potentially affect development of this failure pattern is identified to be the post-yield response of the longitudinal bars across the wall thickness, generating different values of residual strains and consequently inducing their asynchronous yielding under compressive actions. Analytical models proposed in literature for prediction of out-of-plane instability failure as well as their relevant assumptions are compared with the test measurements. While the observations presented in past research on development of out-plane instability in concrete columns representing the boundary zones of rectangular walls are in line with the sequence of events observed in this study, the assumptions made in the analytical models regarding the height of the wall effectively involved in formation of out-of-plane deformations (effective buckling height) were found to be different.

KEYWORDS: rectangular RC walls; out-of-plane instability; in-plane loading; experimental observations

1. INTRODUCTION

According to the observations made in recent earthquakes in Chile and New Zealand, lateral instability of a large portion of rectangular walls (also referred to as out-of-plane buckling) was one of the failure patterns that raised concerns about performance of shear wall buildings designed using modern codes [1]. Prior to the Chile earthquake, this failure mechanism had only been primarily observed in laboratory tests [2-4]. Out-of-plane buckling or instability due to in-plane loads refers to buckling of an end region of a wall section where development of large tensile strains followed by a load reversal can result in exertion of large compressive actions on reinforcing bars of a cracked section, thus providing a critical situation for instability of the section. This failure mode (i.e. instability) can be exacerbated by any inherent eccentricities in the load application in addition to non-uniformity of material response (e.g., reinforcement yielding) along the wall thickness.

Paulay and Priestley [5] made recommendations for the prediction of the onset of out-of-plane instability, based on the observed response in tests of rectangular structural walls and theoretical considerations of fundamental material and structural behaviours. Because of the limited available experimental evidences, engineering judgement was relied on extensively in making these recommendations. The major source of the instability was postulated to be the previously experienced (maximum) tensile strain imposed on the wall rather than the maximum compression strain.

In literature, the out-of-plane instability of rectangular RC walls under in-plane loading has been mainly investigated by idealizing the boundary region of the wall as an axially loaded column. For this purpose, RC prism units were subjected to tension and compression cyclic loading. This type of research on out-of-plane instability failure was first conducted by Goodsir [4] and the main finding was the effect of the maximum tensile strain reached in the reinforcement on development of out-of-plane deformations. Chai and Elayer [6] also conducted an experimental study to examine the out-of-plane instability of several RC columns designed to represent the end-regions of a ductile

[1] Research Engineer (Post-doctoral Researcher), Department of Civil and Natural Resources Engineering, University of Canterbury, Christchurch 8140, New Zealand. E-mail: farhad.dashti@canterbury.ac.nz

[2] Professor, Department of Civil and Natural Resources Engineering, University of Canterbury, Christchurch 8140, New Zealand. E-mail: rajesh.dhakal@canterbury.ac.nz

[3] Professor, Department of Civil and Natural Resources Engineering, Univ. of Canterbury, Christchurch 8140, New Zealand. E-mail: stefano.pampanin@canterbury.ac.nz; Professor, Department of Structural and Geotechnical Engineering, Sapienza University of Rome, Italy. E-mail:stefano.pampanin@uniroma1.it

planar RC wall under large amplitude reversed cyclic tension and compression. Based on this study, the critical influence of the maximum tensile strain on the lateral instability of slender rectangular walls was confirmed and the basic behaviour of the wall end-regions under an axial tension and compression cycle was described by axial strain versus out-of-plane displacement and axial strain versus axial force plots. Also, based on a kinematic relation between the axial strain and the out-of-plane displacement, and the axial force versus the axial strain response, a model was developed for the prediction of the maximum tensile strain. The effect of the specimen thickness was studied in this research, as well. Creagh et al. [7] and Chrysanidis and Tegos [8] subjected concrete prisms to tension and then compression until failure. The results of these experiments confirmed the effect of maximum tensile strain developed during the tensile loading on out-of-plane instability of the specimen during unloading and the compressive loading. In another test campaign by Shea et al. [9], the influence of specimen thickness as well as the maximum tensile strain was investigated. Rosso et al. [10] studied the parameters affecting the out-of-plane response of singly reinforced walls using cyclic tensile-compressive tests on the corresponding boundary elements. Haro et al. [11] included bi-directional loading protocols in the RC prism testing and scrutinized the effect of the longitudinal reinforcement ratio on the onset of out-of-plane instability in planar walls.

Investigating the out-of-plane instability by testing idealized columns representing boundary zones of rectangular walls may be an efficient approach for conducting parametric studies compared to testing a whole wall unit. However, the following features affecting this mode of failure are not accounted for in this approach [12]:

1- The wall region that undergoes out-of-plane instability is not limited to the end boundary zone, and there is no clear definition of this region and its relationship with the longitudinal reinforcement layout.
2- The effect of boundary conditions (top and bottom connections as well as the connection of one side of the boundary region to the web region) and the strain variation along the wall height are not taken into account.
3- The assumption of plastic hinge length as the length involved in the formation of out-of-plane deformation (effective buckling height) needs to be validated.

Rosso et al. [12] studied the out-of-plane failure mode of walls by investigating the measured response of two singly reinforced T-shaped walls tested under cyclic loading. The specimens were identical but were subjected to two different in-plane and bi-directional loading patterns. However, the authors are not aware of any tests on doubly reinforced walls addressing the mechanism of out-of-plane instability failure in rectangular walls.

In this study, the development of out-of-plane instability in rectangular walls is investigated by analyzing the response of a doubly reinforced wall specimen designed according to the New Zealand concrete standard NZS3101:2006 and subjected to in-plane cyclic loading. Out-of-plane instability was the primary failure pattern of this specimen, and its response was not influenced by other failure patterns such as bar buckling. Therefore, the observations and measurements made in this test at different stages of loading are used to scrutinize the mechanism of out-of-plane instability and the controlling parameters. For this purpose, the maximum tensile strain variations along the height of the boundary zone are extracted and compared with the measured out-of-plane displacement profile of the specimen and the observed effective buckling height. These measurements are compared with the predictions and assumptions of the analytical models proposed in literature for prediction of out-of-plane instability. Particularly, the sequence of events observed and presented by Chai and Elayer [6] regarding development of out-plane instability in concrete columns representing the boundary zones of rectangular walls are compared with the observations of this experimental study and the assumption of plastic hinge length as the length involved in the formation of out-of-plane deformation (effective buckling height) is evaluated.

It should be noted that the authors have numerically scrutinized development of out-of-plane deformation and the subsequent instability in rectangular structural walls and tested several specimens for parametric investigation of this failure pattern [13-16]. The response of one specimen, whose results were found to be best suited to highlight in great details the evolution of out-of-plane deformation and instability, is discussed herein. The findings presented in this study are not in conflict with any of the several other walls the authors have investigated.

2. MODELS FOR PREDICTION OF OUT-OF-PLANE INSTABILITY

Paulay and Priestley [5] scrutinized the mechanism of out-of-plane instability by idealization of the part of the wall height that has undergone out-of-plane deformation with a circular shape, as shown in Figure 1. Δl_o in this figure is the elongation of the vertical reinforcement due to previously imposed residual strains, i.e., $\Delta l_o = \varepsilon_{sm} l_o$. By expressing the lateral displacement δ in terms of the wall thickness b, i.e., $\delta = \xi b$, and using expressions developed for estimation of the radius of curvature, the eccentricity ratio ξ was calculated as:

$$\xi = \frac{\varepsilon_{sm}}{8\beta}\left(\frac{l_o}{b}\right)^2 \quad (1)$$

where

ε_{sm}= the maximum tensile strain of the longitudinal reinforcement (the relatively small elastic recovery was neglected and the residual strain was assumed to be of the order of ε_{sm}).
l_o = the height along which out-of-plane instability develops and assumed to be equal to the theoretical length of the plastic hinge
βb = the distance from the layer of elastic reinforcement to the point of initial crack closure (Figure 1).
In order to establish a stability criterion for the section undergoing out-of-plane deformations, the section equilibrium was used (Figure 1).

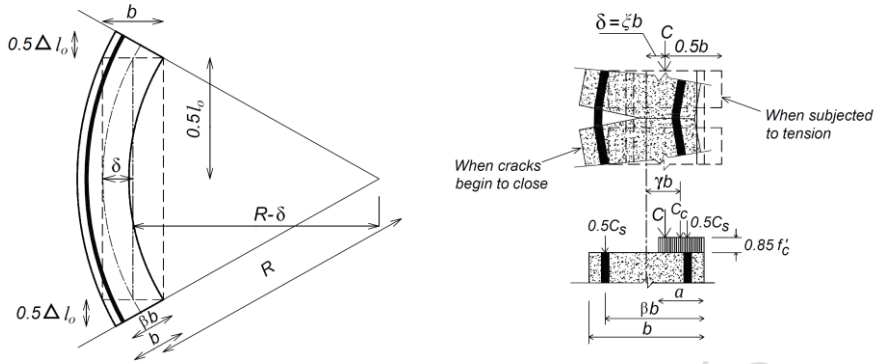

Figure 1. Geometry of buckling and relation of internal forces to eccentricity (adapted from Paulay and Priestley [5])

According to Paulay and Priestley [5], out-of-plane instability of the section will occur if the lateral displacement exceeds half of the wall thickness. The equilibrium of the section shows that the compression force (C) applied with an eccentricity of $\delta = \xi b$ is sustained by the compressive actions of the reinforcement as well as some concrete compression force C_c within the crack closure area. It is assumed that all bars develop yield stress f_y at partial crack closure although the two layers of reinforcement would undergo different values of compressive strains. The following equation was derived using the equilibrium equations and considering the assumption of the equivalent rectangular compression stress block

$$\gamma = \frac{1}{2}\left[(\xi + 0.5) - \sqrt{(\xi + 0.5)^2 - 2\xi(1 + 1.176m)}\right] \quad (2)$$

where
$m = \rho f_y / f_c'$
γb = lever arm of the force C_c with respect to the wall centerline (Figure 1).
As the term inside the square root sign needs to be nonnegative, the stability criterion of the wall section was derived as

$$\xi \le \xi_c = 0.5(1 + 2.35m - \sqrt{5.53m^2 + 4.70m}) \quad (3)$$

Chai and Elayer [6] studied the out-of-plane instability of ductile RC walls by idealizing the end-region of the wall as an axially loaded RC column, and conducted an experimental study to examine the out-of-plane instability of several RC columns designed to represent the end-regions of a ductile planar RC wall under large amplitude reversed cyclic tension and compression.
Based on this study, the critical influence of the maximum tensile strain on the lateral instability of slender rectangular walls was confirmed and the basic behaviour of the wall end-regions under an axial tension and compression cycle was described by axial strain versus out-of-plane displacement and axial strain versus axial force plots shown in Figure 2. Also, based on a kinematic relation between the axial strain and the out-of-plane displacement, and the axial force versus the axial strain response, a model was developed for the prediction of the maximum tensile strain. Points *a-f* display different stages of the idealized column response, which are briefly described in Table 1.
Chai and Elayer [6] used the same stability criterion as Equation 3 and considered three components for ε_{sm} as:

$$\varepsilon_{sm} = \varepsilon_e + \varepsilon_r + \varepsilon_a^* \quad (4)$$

$$\varepsilon_{sm} = \eta_1 \varepsilon_y + \eta_2 \varepsilon_y + \varepsilon_a^* \quad (5)$$

1) ε_e= an elastic strain recovery for the unloading from a tensile excursion;
2) ε_r = a reloading strain associated with compression yielding of the reinforcement (and depends on the cyclic characteristic of the reinforcing steel since a reduced stiffness in the steel is expected due to the Bauchinger'strain effect)
3) ε_a^* = an axial strain at first closure of cracks

Based on the relationship of the transverse curvature at mid-height of the column with the mid-height out-of-plane displacement and axial strain corresponding to the first crack closure the following kinematic relation was derived:

$$\varepsilon_a^* = \left(\frac{1}{2c}\right)\left(\frac{b}{l_o}\right)^2 \xi_m \tag{6}$$

where, c depends on the transverse curvature distribution of the column and ξ_m is the out-of-plane displacement at mid-height of the column, as normalized by the wall thickness.

The following assumptions were made:

- The out-of-plane displacement for the crushing limit state (i.e., Point *e* in Figure 2) was assumed to be fairly close to the out-of-plane displacement at first crack closure i.e., Point *d* in Figure 2.
- The limit state for calculation of the out-of-plane displacement was concrete crushing. i.e. ξ_c is the out-of-plane displacement corresponding to the concrete crushing and the out-of-plane displacement should be limited to ξ_c.
- η_1 = 1.0, and η_2 = 2.0
- The curvature distribution was considered sinusoidal, i.e., coefficient $c = 1/\pi^2$

Based on these assumptions, the maximum tensile strain that may be imposed on the longitudinal reinforcement was written as

$$\varepsilon_{sm} = \frac{\pi^2}{2}\left(\frac{b}{l_o}\right)^2 \xi_c + 3\varepsilon_y \tag{7}$$

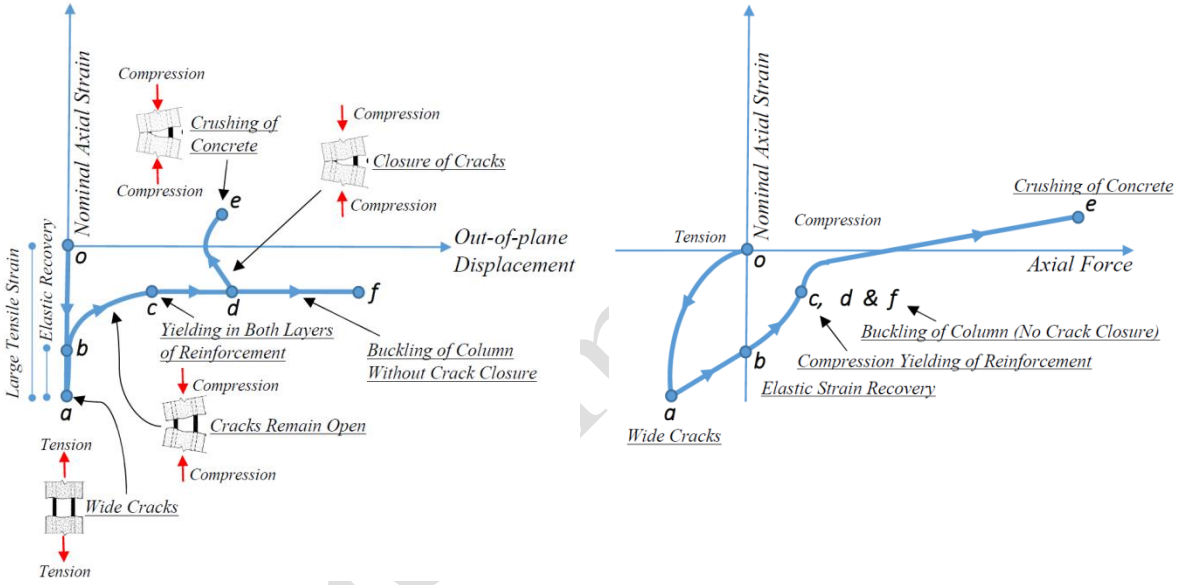

(a) (b)

Figure 2. Axial reversed cyclic response of RC column: (a) nominal axial strain versus out-of-plane displacement; and (b) nominal axial strain versus axial force (adapted from Chai and Elayer [6])

Table 1. Behavior of wall end-region under the loading cycle shown in Figure 2

	Path	
Loading	*o-a*	Large tensile strain
Unloading	*a-b*	Elastic strain recovery mainly in reinforcing steel
Reloading	*b-c*	Reloading in compression on the cracked concrete column accompanied by an out-of-plane displacement; yielding of the reinforcement closer to the applied axial force resulting in a reduced transverse stiffness of the column and an increased out-of-plane displacement.
	c-d	Compression yielding in the second layer of the reinforcement, and a rapid increase in the out-of-plane displacement
	d-e	Closure of cracks at Point d and decrease of out-of-plane displacement and increase of out-of-plane displacement after significant compressive strain is developed in the compressed concrete
	d-f	An excessive crack opening where subsequent compression would not result in the closure of the cracks but a continued increase in the out-of-plane displacement and eventual buckling of the column

The authors [13-16] numerically investigated the progression of out-of-plane deformation and subsequent instability observed in several singly and doubly reinforced wall specimens under concentric in-plane cyclic loading. The evolution of this failure pattern was scrutinized by analyzing the stress and strain gradients of the reinforcement and concrete elements along the length, height and thickness of the numerical model generated for one of the specimens

[15, 17, 18]. The sequence of events leading to formation of out-of-plane instability in the numerical model was in line with prior research findings (i.e. Paulay and Priestley [5] and Chai and Elayer [6]) and it was confirmed that the out-of-plane deformation is triggered by the maximum strain reached by reinforcement elements in the previous cycles.

The stages of development of out-of-plane instability that were predicted by the numerical model comprised of two basic scenarios: 1) evolution followed by full or partial recovery of out-of-plane deformation, and 2) evolution of out-of-plane deformation leading to out-of-plane instability. These two scenarios are depicted in Figure 3 (C1-a to C1-c representing Scenario 1 and C2-a to C2-c representing Scenario 2). The loading stage corresponding to each phase is displayed. The response of the wall boundary region at the elevation corresponding to the maximum out-of-plane displacement is shown schematically in terms of stresses in the concrete and reinforcement on the territory of a single crack. The letters "T" and "C" correspond to tensile and compressive stresses, respectively. These schematics will be used hereafter for representation of the stages shown in Figure 3. Note that the deformation patterns are exaggerated in this figure for better illustration of the local response.

At large in-plane curvature demands (C1-a and C2-a, Figure 3), large residual tensile strains can readily lead to development of larger compressive stresses in the reinforcement prior to crack closure during the load reversal. Once the reinforcing bars yield in compression while the cracks are still open, deformation of the wall in the out-of-plane direction is inevitable. However, depending on the initial tensile strain different scenarios can occur. If the initial tensile strain is small, crack closes early in the inner face (C1-b, Figure 3) which enables the concrete to contribute to the load carrying capacity of the section; thereby leading to the recovery of the out-of-plane deformation (C2-c, Figure 3). Depending on the initial tensile strain and some other parameters (such as axial load), the extent of this recovery may vary, leaving no or a specific amount of residual out-of-plane deformation. On the contrary, if the applied drift level imposes larger initial tensile strains (C2-a, Figure 3), the crack closure may not initiate before progression of significant out-of-plane deformation (C2-b, Figure 3) leading to instability of the wall (C2-c, Figure 3).

An experimental campaign was conducted by the authors for further verification of the mechanism of out-of-plane instability predicted by the numerical model and to experimentally investigate the parameters controlling this failure pattern. However, comparison of the numerical predictions versus experimental observations and the results of the parametric study are not included in this paper. Nevertheless, the response of one specimen, whose results were found to be best suited to highlight the evolution of out-of-plane deformation and instability, is presented in detail herein.

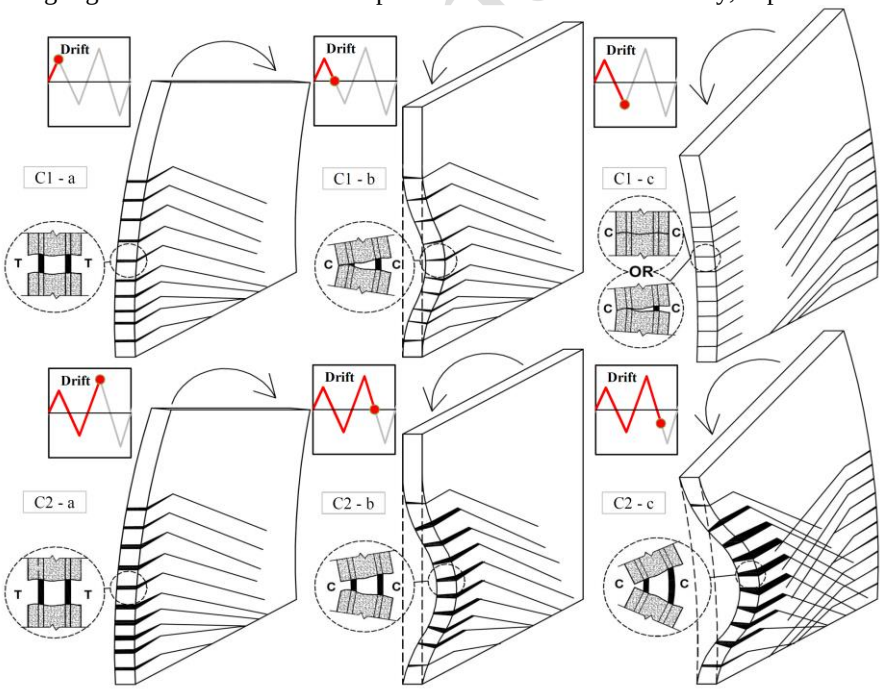

Figure 3: Evolution and recovery of out-of-plane deformation (C1-a to C1-b); formation of out-of-plane instability (C2-a to C2-c)

3. EXPERIMENTAL PROGRAM

Figure 4 displays the geometry and reinforcement configuration of the specimen. The test specimen was a half-scale model, representing the first story of a four-storey high wall. The unsupported height of the specimens was 2.0 m;

thereby representing a storey height of 4.0 m. The test setup was thus designed to apply the lateral load as well as the axial load and bending moment coming from the upper stories producing a shear-span of 6.0 m. Figure 5a displays the configuration of horizontal and vertical actuators producing this loading pattern. As movements of the horizontal and vertical actuators were interdependent, a control program was designed to balance the actuators at each step through an iterative approach so that they complied with the above mentioned loading conditions and satisfied the design shear-span ratio. The specimen was connected to the loading beam by two steel angles bolted to the wall panel through embedded threaded rods and to the loading beam by high strength bolts. The loading beam was restrained against out-of-plane displacement using roller supports, as shown in Figure 5b. A load cell was attached to each roller to measure the variations of the out-of-plane load at different stages of loading (Figure 5b). These roller supports were positioned on both sides and at different elevations of the loading beam to restrain the rotation of the loading beam and consequently of the top of the specimen, representing the restraints at the storey level of a structural wall connected to the floor system in a building (Figure 5c). The specimen was subjected to a quasi-static cyclic loading regime with three cycles at each drift level and an axial load ratio of 0.06. Figure 6 displays the displacement history of the control point, located at elevation of 2.0 m from the wall base, which was used to control the horizontal actuator (Figure 5a). The loading applied by the vertical actuators consisted of the axial load and the bending moment corresponding to each increment of the lateral displacement.

In order to capture the average strain of reinforcement along the area which was assumed to be more prone to out-of-plane deformations, linear potentiometers had been used in the test. These potentiometers were connected to the rebars using welded couplers. In order to capture the out-of-plane deformations, string potentiometers were positioned along the height of both boundary regions and up to the height of 1230 mm from the base of the specimen. In order to monitor the variations of strain throughout the wall panel and along the wall thickness at different stages of loading, in addition to the potentiometers that were welded to the reinforcement, reinforcement strain gauges and linear potentiometers attached to the concrete core were also used. The strain gauges were attached to both layers of reinforcement at some locations along the height of the boundary zones. The strain measurements captured using the instrumentation mentioned above have been compared to cross-check the readings. The strain gauge measurements were in good agreement with the data captured by the potentiometers attached to the reinforcement for all drift levels indicating that the measurements were reliable. The average strain captured by the potentiometers that were attached to the concrete core provided a good matching with the reinforcement strain measurements which is a sign of minimal bond-slip between concrete and reinforcement in this specimen until 3.0% drift level. The instrumentation is described in more detail in [13] and [19].

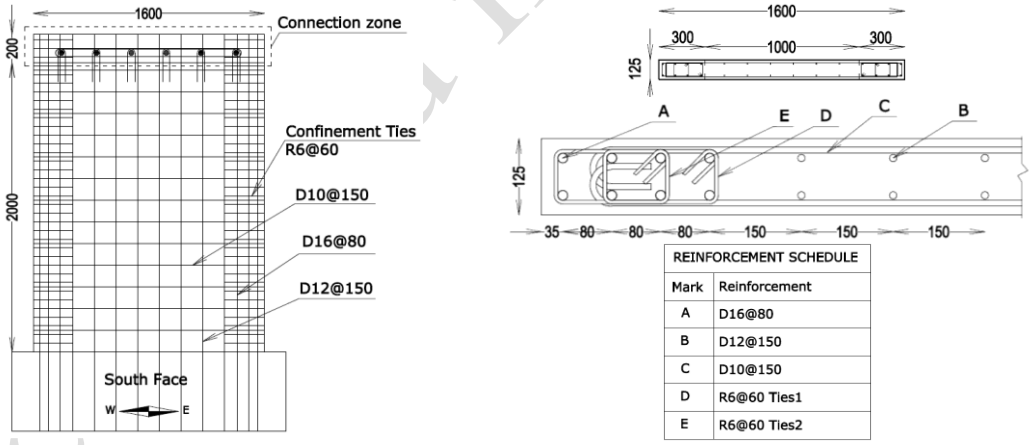

REINFORCEMENT SCHEDULE	
Mark	Reinforcement
A	D16@80
B	D12@150
C	D10@150
D	R6@60 Ties1
E	R6@60 Ties2

Figure 4. Geometry and reinforcement configuration of the specimen

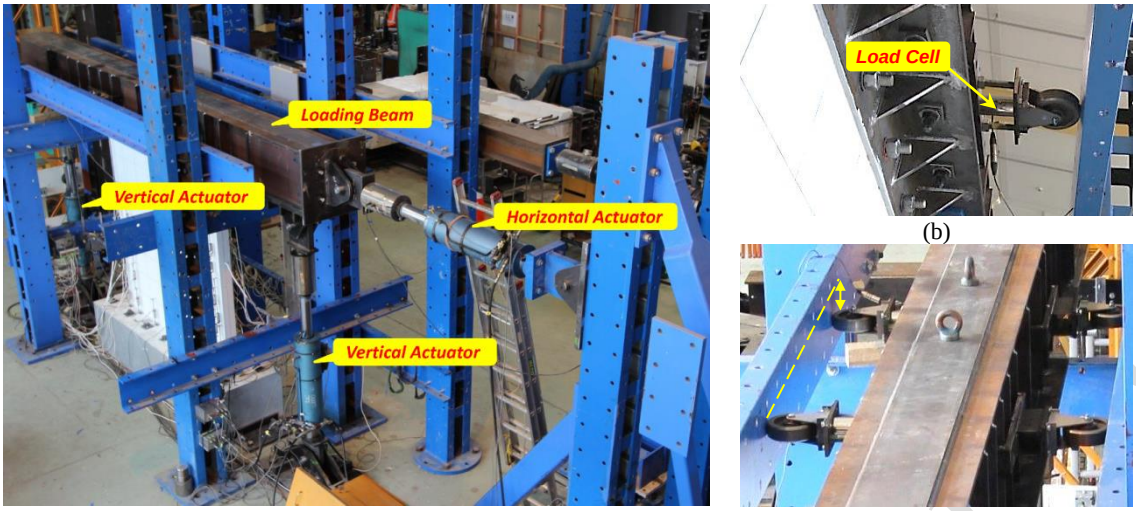

Figure 5. Test setup: (a) configuration of the actuators; (b) connection details of the loading beam and the roller supports; (c) roller supports positioned on both sides at different elevations of the loading beam

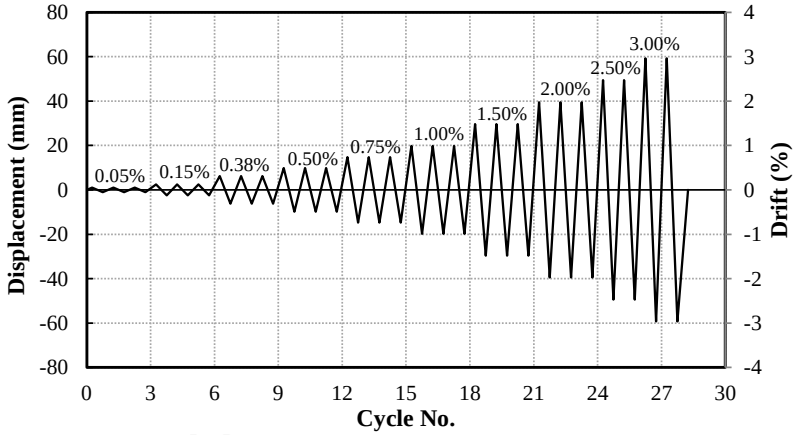

Figure 6. Displacement history (The specimen failed during the 1st cycle of the 3.0% drift)

4. SPECIMEN RESPONSE

Figure 7a displays the lateral load versus top displacement response of the specimen. Out-of-plane instability was the primary failure pattern of the specimen and neither bar fracture nor bar buckling was observed in the test. Out-of-plane deformation developed in both boundary regions during testing and the specimen failed when the west boundary region exhibited a considerably large out-of-plane displacement. The out-of-plane displacement of this boundary region measured by an instrument positioned at elevation of 600 mm from the base versus top displacement of the specimen is also plotted in Figure 7a. Figure 7b indicates the extent of out-of-plane displacement developed in the west boundary region at Point B and Figure 7c shows the failed specimen.

The out-of-plane deformation initiated at Point A when the specimen was unloaded from the positive peak of the 1.5% drift cycle and was starting to reload in the opposite direction. As can be seen in Figure 7a, the out-of-plane deformation recovered completely as the specimen was re-loaded in the opposite direction. This out-of-plane displacement recovery occurred at early stages of loading. When the specimen was subjected to the 2.5% drift cycles, it started to exhibit residual out-of-plane displacement. The residual out-of-plane displacement increased with the number of cycles and the specimen became unstable at Point B where an abrupt strength degradation was observed.

Figure 8 displays visual progression of out-of-plane deformation in the west boundary region during the 2nd 2.5% drift cycle and occurrence of out-of-plane instability during the 1st 3.0% drift cycle together with the lateral load vs top displacement response of the specimen and the evolution of maximum out-of-plane displacement in the west boundary region during these two cycles (Figure 8i). Reinforcement strain at different stages of loading, unloading and reloading has been identified as one of the main parameters controlling out-of-plane deformations of rectangular walls. As the strain gauges exceeded their limited range of functionality before reaching this stage, the average strain of the end

region bars was calculated using measurements of the linear potentiometers that were welded to these bars and plotted against the out-of-plane displacement response of the west boundary in Figure 8ii. This figure is presented in the same style as Figure 2a for easier comparison of the failure model proposed by Chai and Elayer [6] based on axially loaded columns with the evolution of out-of-plane instability in rectangular walls under in-plane seismic loading. Points a1-f1 and a2-f2 in Figures 8i and 8ii correspond to Figures 8a1-f1 and Figures 8a2-f2, respectively. The test photos corresponding to Points b1 and b2 are not displayed.

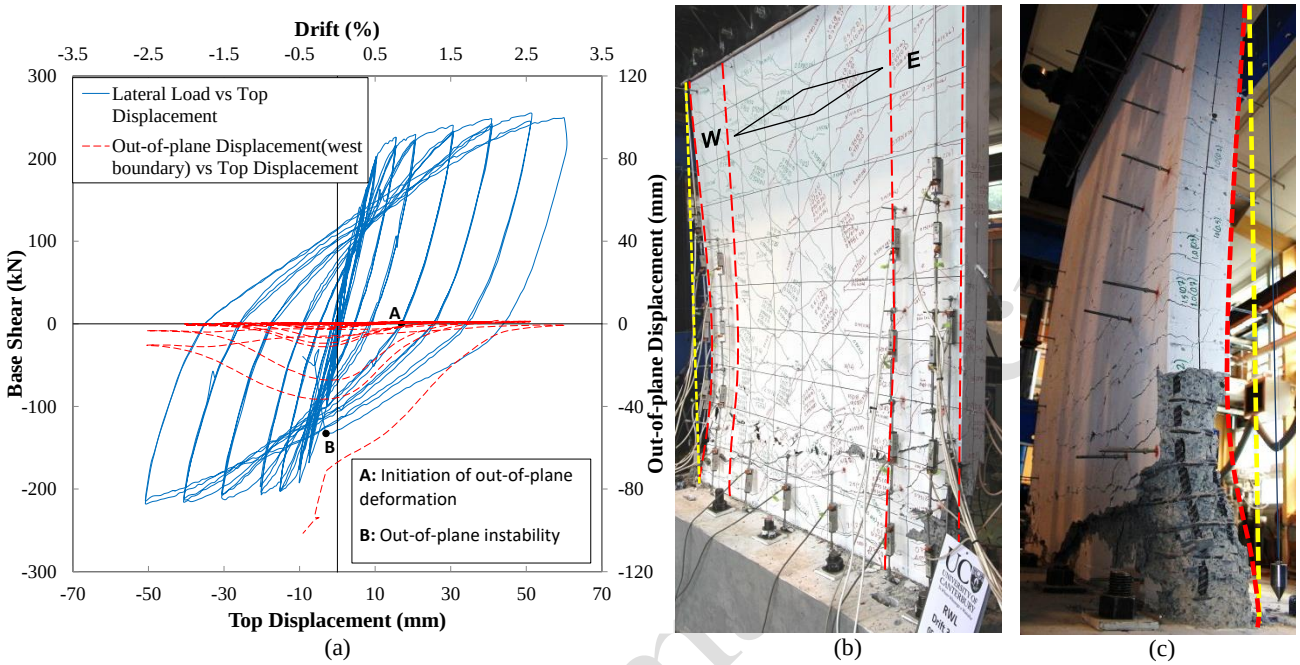

Figure 7. Response of the specimen: (a) lateral load vs top displacement response of the wall and out-of-plane response of the west boundary; (b) south face – prior to instability at Point B (dashed lines show the extent of the boundary regions); (c) west boundary zone – after instability at Point B

Figures 8 (a1-e1) display the formation of out-of-plane deformation in the west boundary region during the second cycle of 2.5% drift level. Figure 8a1 indicates the wide cracks in the boundary region before initiation of out-of-plane displacement at 2.5% drift cycle. Figure 8b1 displays development of the out-of-plane deformation at this drift level. Figure 8c1 indicates the maximum out-of-plane deformation (as also shown in Figures 8i and 8ii) and initiation of crack closure in one (i.e. inner) face of the wall. This crack closure resulted in decrease of the out-of-plane deformation in the following stages (Figure 8d1) and its recovery (Figure 8e1). The out-of-plane deformation did not recover completely at this stage (Point f1, Figure 8ii) leaving some residual out-of-plane displacement in the west boundary region. As can be seen in Figure 8i, development and recovery of out-of-plan deformation, denoted as Path a1-b1-c1-d1-e1-f1, did not have any influence on the lateral load vs top displacement curve of the specimen although a maximum out-of-plane displacement of about 40 mm was generated in the west boundary region.

The out-of-plane deformation increased in the east boundary element as well when the specimen was being unloaded and reloaded in the positive direction toward 3.0% drift level. The out-of-plane displacement response of this boundary region and its relationship with the average strain of the corresponding end region bar is indicated in Figure 9. In the east boundary region, the trend was quite similar to the one in the west boundary at 2.5% drift cycle except that the loading of the specimen towards +3.0% drift level after recovery of the out-of-plane displacement resulted in concrete crushing in the inner face at the section with maximum out-of-plane deformation, and the out-of-plane displacement increased at Point *e*. Had the loading continued in the same direction, the out-of-plane displacement could have increased steadily resulting in instability of the specimen.

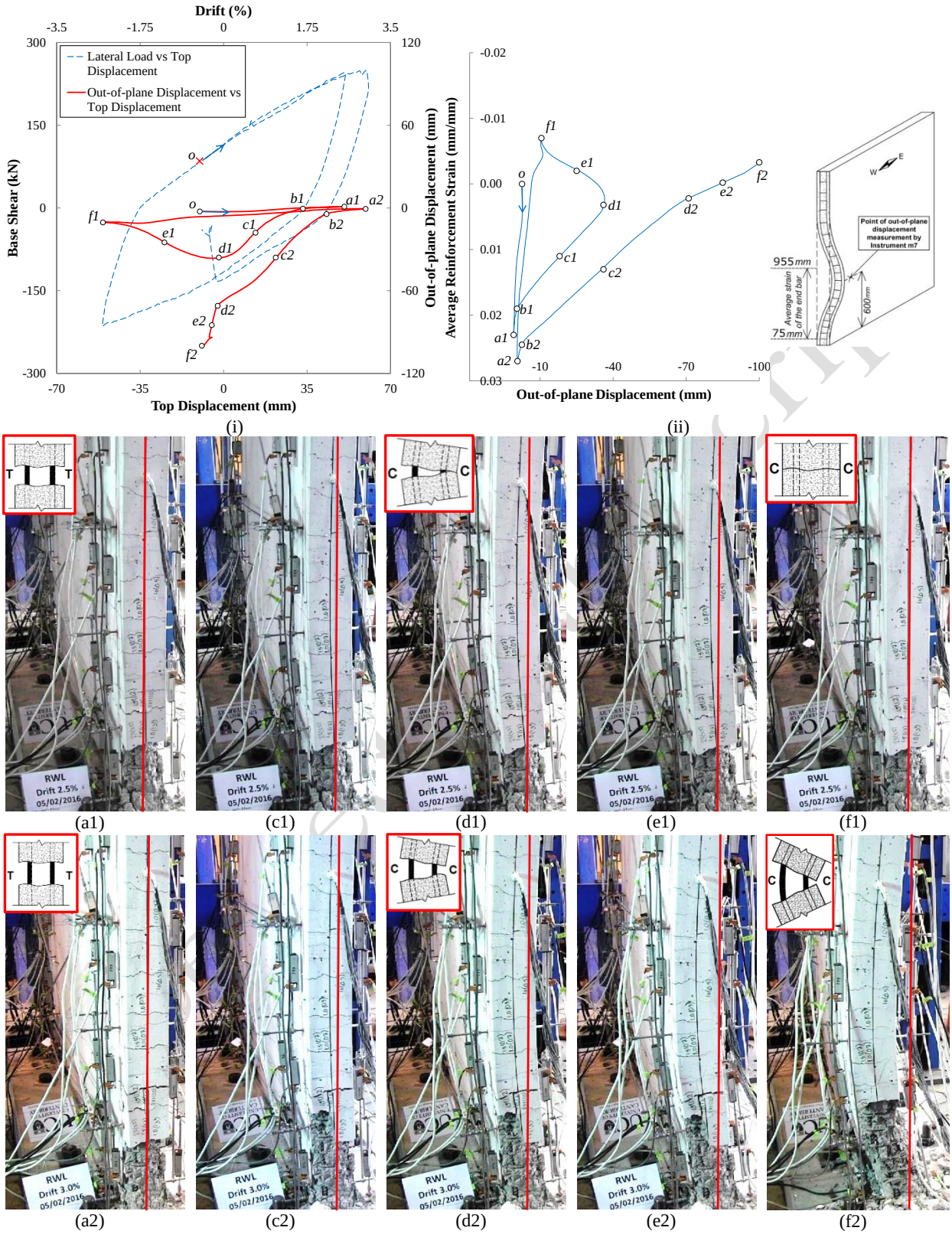

Figure 8: (i) Out-of-plane displacement response of the west boundary during the 2nd cycle of 2.5% and the 1st cycle of 3.0% drift; (ii) average strain of the end region bar vs maximum out-of-plane displacement response of the west boundary for these two cycles; (a1-f1) development and recovery of out-of-plane deformation in the west boundary region, 2nd cycle of 2.5% drift; (a2-f2) occurrence of out-of-plane instability,1st cycle of 3.0% drift

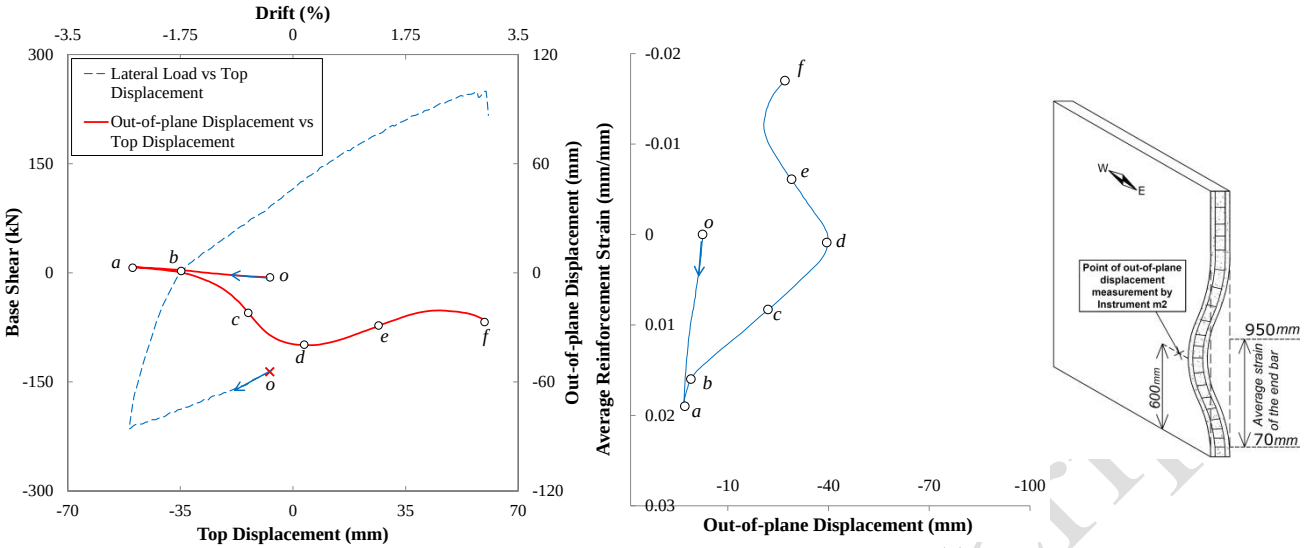

Figure 9: (i) Out-of-plane displacement response of the east boundary during the 2nd cycle of 2.5% and the 1st cycle of 3.0% drift; (ii) average strain of the end region bar vs maximum out-of-plane displacement response of the east boundary for these two cycles

During unloading from +3.0% drift level and reloading towards -3.0% drift level, the out-of-plane deformation increased in the west boundary region. However, as the cracks generated in this boundary region during +3.0% loading were wider than the previous cycle at 2.5% drift level, the cracks did not fully close and the out-of-plane deformation increased steadily leading to out-of-plane instability of the wall. Figures 8a2-f2 display the formation of out-of-plane instability which can be compared with Figures 8 (a1-f1), the stage where timely crack closure resulted in recovery of the out-of-plane deformation. Figure 8f2 corresponds to out-of-plane instability of the specimen and the abrupt strength degradation during Path d2-f2 (in Figure8 i) is due to this instability.

The aforementioned steps leading to formation of out-of-plane deformation and out-of-plane instability are in line with the postulations described by Paulay and Priestley [5], and results of the experiments conducted by Chai and Elayer [6] (Figure 2, Table 1). As can be seen in Figure 2 and Table 1, the reloading in compression of the idealized column could be either Path *b-c-d-e* or Path *b-c-d-f*. Response of the specimen's east boundary region when unloading from 2.5% drift level and reloading to 3.0% drift (Figure 9) represents Path *b-c-d-e* (Figure 9ii compared to Figure 2) and the evolution of out-of-plane instability in the west boundary illustrated in Figures 8a2-f2 represents Path *b-c-d-f* (Figure 8ii compared to Figure 2). Also, the sequence of events observed in the experiment matches well with the development of out-of-plane instability simulated by the numerical modeling approach investigated by the authors (Figure 3). The stages corresponding to evolution and recovery of the out-of-plane displacement (Figures 8a1-f1 compared to Path C1-a to C1-c of Figure 3) and formation of out-of-plane instability (Figures 8a2-f2 compared to Path C2-a to C2-c of Figure 3), as well as their relationship with the reinforcement and concrete response, match well with the trend predicted by the numerical model [13-16].

The following sequence of events observed in the tested specimen can therefore be confirmed, which is also in good agreement with the findings and postulations of the relevant studies available in the literature:

a) Development of large tensile strains in the longitudinal reinforcement of the specimen led to generation of significant compressive stresses in these bars during loading reversal and resulted in their yielding in compression. This yielding of the longitudinal bars in compression, when occurred along a sufficient height (effective buckling height) and length of the wall, caused a considerable reduction of stiffness in its out-of-plane direction and resulted in movement of the compression zone in this direction.
b) As the out-of-plane deformation increased, cracks started to close on one face of the elevation corresponding to the maximum out-of-plane deformation, which activated load carrying capacity of concrete and resulted in recovery of the out-of-plane deformation (i.e. straightening of the wall) as the loading reversal continued.
c) With this phenomenon being dependent on the residual strain of the longitudinal bars, the out-of-plane deformation grew with the increase in the applied peak drift and the number of cycles per drift level, producing gradually increasing residual out-of-plane deformation in the boundary regions. The wall became unstable when the residual strain of the longitudinal reinforcement was large enough to prevent crack closure prior to the out-of-plane deformation exceeding its critical value equal to half the wall thickness.

As the crack closure on one face of the elevation corresponding to the maximum out-of-plane deformation reestablishes contribution of concrete to the load-carrying capacity of the wall section, the evolution and recovery of

out-of-plane does not cause any strength degradation in the lateral load-top displacement response of the wall. However, when the crack closure does not occur and this deformation increases steadily, an abrupt drop of strength and instability of the whole section is inevitable.

5. VARIATION OF STRAIN ACROSS THE WALL THICKNESS

The effects of eccentricities across the wall thickness associated with material properties, positioning of the longitudinal reinforcement and loading can potentially affect the development of out-of-plane deformation in rectangular walls under in-plane loading. These eccentricities are likely to prevent development of identical tensile and compressive strains across the wall thickness and consequently produce variation of residual strain between two layers of the longitudinal reinforcement. In this section, this phenomenon is investigated by the strain measurements at both layers of the longitudinal reinforcement at the section close to the elevation where the maximum out-of-plane displacement was recorded. Figure 10 shows the strain history of the west boundary extreme end reinforcement at both layers and at the elevation of 560 mm (Strain Gauge 14 for south layer and Strain Gauge 142 for north layer) which is fairly close to the location of the maximum out-of-plane displacement (measurement by instrument m7, Figure 10). The development of the maximum out-of-plane displacement corresponding to each drift cycle is also plotted for better illustration of the relationship between reinforcement strain history and out-of-plane displacement.

Prior to yielding of reinforcement at this elevation (0.5% drift, Figure 10a), the two strain gauges recorded almost identical measurements for both longitudinal bars. After the bars yielded at the elevation of the attached strain gauges (0.75% drift, Figure 10b), the bars located at the same location along the wall length and in two different layers along the wall thickness did not necessarily exhibit exactly alike strain histories as the bar yielding generated eccentricities across the wall thickness. From this drift level onwards, the points corresponding to the elastic strain recovery of the reinforcement are denoted as "*b*". The bars reached different levels of maximum strain at Point *a* and followed the unloading and reloading paths with different strain values. The larger tensile strains of the bars at 1.5% drift cycle resulted in a long distance between the elastic strain recovery and crack closure in terms of residual strain (almost $6\varepsilon_y$), providing ideal circumstances for significantly going beyond yielding in compression at this elevation. With this compression yielding having developed along a sufficient height and length of the wall at this stage, the out-of-plane deformation of the west boundary reached a considerable level during the 1.5% cycle. Different values of maximum and residual tensile strains of the bars (Point *a*, Point *b*, respectively) located at two different positions along the thickness is quite noticeable at this stage and could have potentially induced eccentricities across the wall thickness in terms of compressive yielding of the longitudinal bars. A similar trend was observed at 2.0% drift level (Figure 10e). At this drift level, the maximum tensile strain was not recorded after reaching 0.02 which seems to be the maximum level of measurable strain by this type of strain gauges.

Figure 11 displays the average strain profiles along the height of the west boundary region and on both faces of the specimen calculated using the measurements of the corresponding potentiometers. These instruments were anchored deep enough into the concrete to measure the displacement values of concrete at the same position as the reinforcement along the thickness. However, they had to be positioned slightly far from the extreme end reinforcement along the wall length and may not represent the concrete response at the same level along the length as the extreme end reinforcement. The average strain measurements are plotted at mid-height of the corresponding instrument in Figure 11 with linear variation between two readings to facilitate illustration of the strain variations at different drift levels in a single figure. The strain values represented post-yielding (0.75% drift onwards) state of the specimen. As can be seen in Figure 11, the maximum tensile strains along the height of the north and south faces of the west boundary region are different. This asymmetric tensile vertical strain along the thickness at 1.5% could have played its part on eccentricity of the wall section during unloading and reloading stages resulting in initiation of the out-of-plane deformation.

The difference between the maximum tensile strains developed in the bars of different layers of longitudinal reinforcement would consequently cause variation in the corresponding residual strains. During the phase when the cracks are wide open and the compression is resisted solely by reinforcement, this variation would generate an eccentricity along the wall thickness by inducing earlier onset of compressive yielding in one layer of the longitudinal reinforcement with respect to the other layer and trigger initiation of the out-of-plane deformation.

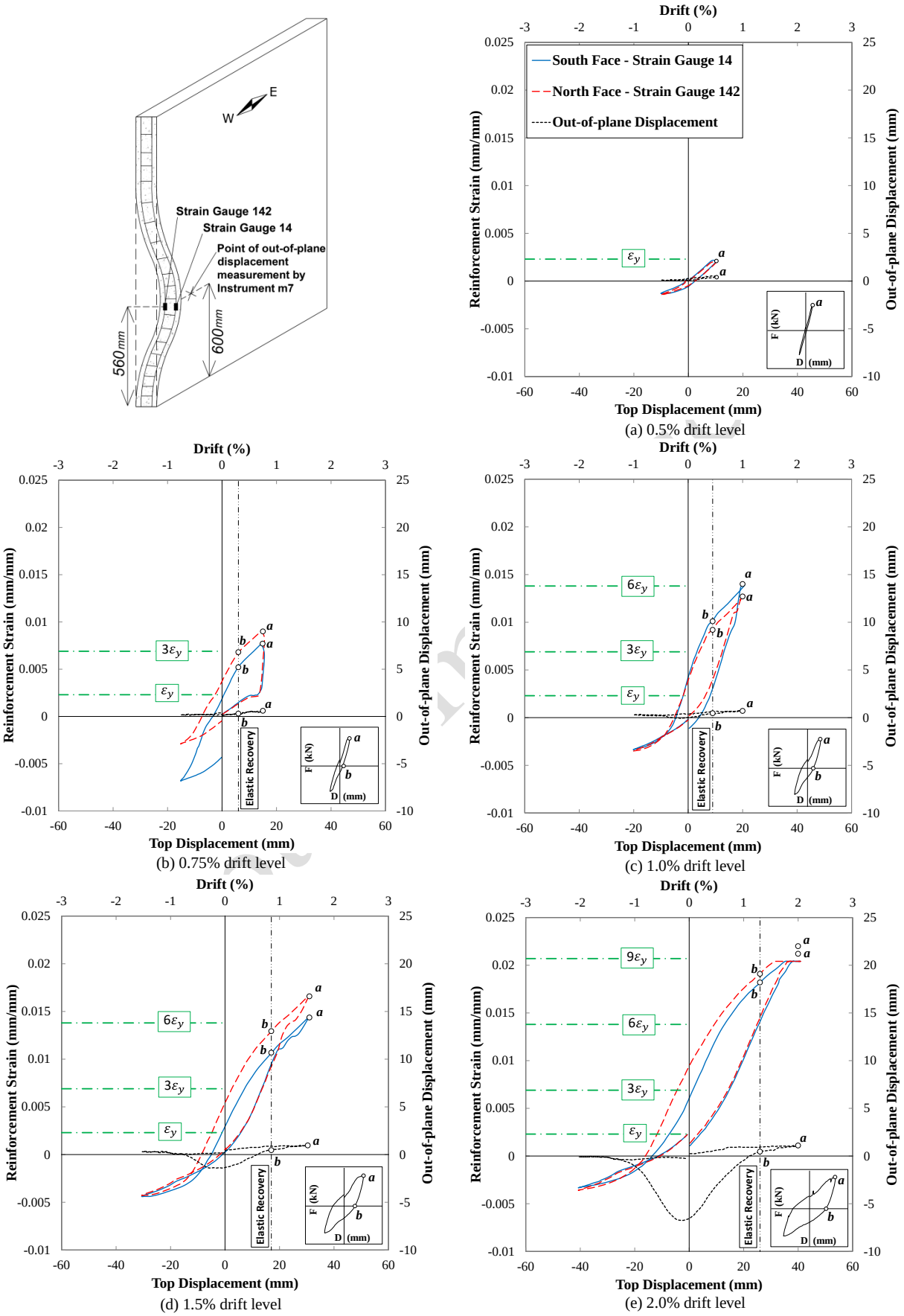

(a) 0.5% drift level

(b) 0.75% drift level

(c) 1.0% drift level

(d) 1.5% drift level

(e) 2.0% drift level

Figure 10. Response of the west boundary extreme end reinforcement at 560 mm from the base

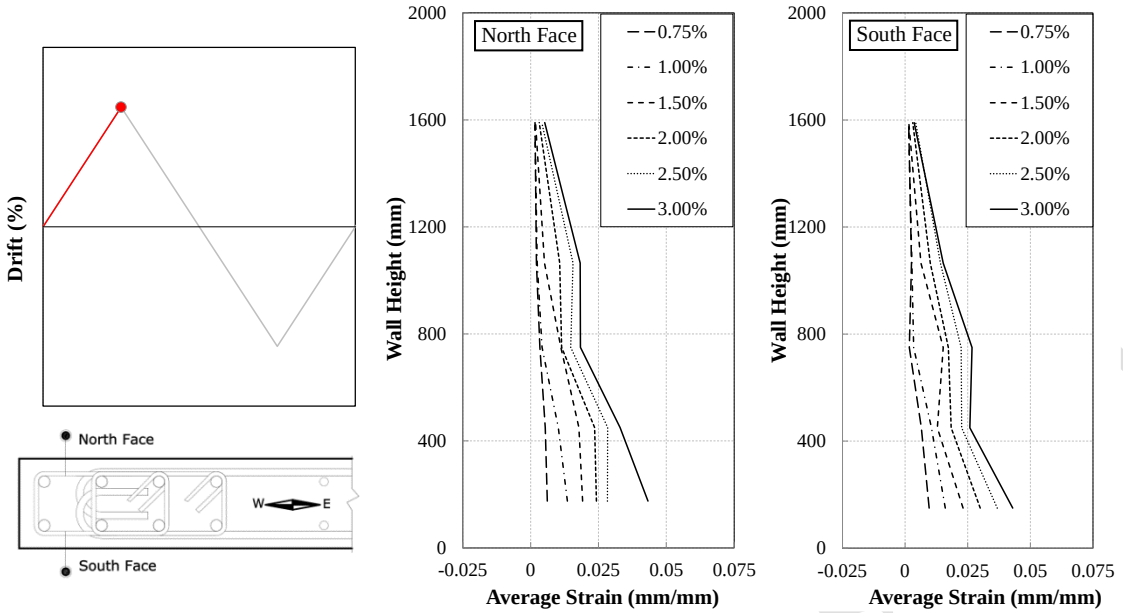

Figure 11. Average strain along the height and on both faces of the west boundary region corresponding to peak positive drift levels

6. COMPARISON OF RESULTS WITH EXISTING ANALYTICAL MODELS AND THE EFFECTS OF PREVIOUSLY IMPOSED TENSILE STRAIN GRADIENTS

In this section, the experimental observations and measurements regarding initiation and development of out-of-plane deformation and evolution of out-of-plane instability are compared with the predictions and assumptions of the analytical models proposed in literature for prediction of this failure pattern in rectangular walls. Figure 12 displays the maximum out-of-plane displacement measured at boundary zones, as normalized by the wall thickness ($\xi = \delta/b$), versus the in-plane top displacement of the specimen.

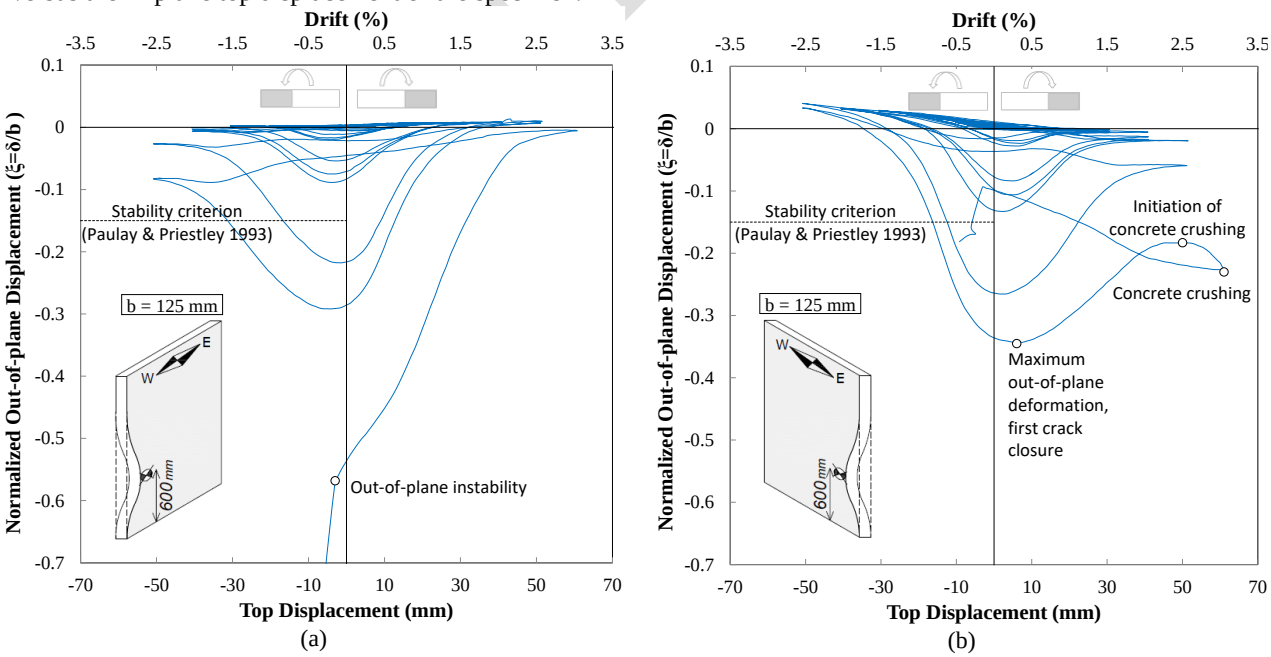

Figure 12. In-plane top displacement versus normalized maximum out-of-plane displacement: (a) west boundary region; (b) east boundary region

As can be seen in Figure 12a, the out-of-plane deformation in the west boundary region increased during unloading from the peak drift and going back through the original undeformed position (0.0% drift) at different cycles. The out-of-plane displacement recovered up to a certain level at different drift cycles until 3.0% drift, where instead of

recovering, the out-of-plane deformation increased steadily after reaching the maximum value and resulted in instability of the specimen. Paulay and Priestley [5] proposed that the out-of-plane displacements exceeding half of the wall thickness (i.e. $\xi > 0.5$) would definitely result in instability of the wall. The normalized out-of-plane displacement prior to instability of the specimen was measured as $\xi = -0.57$ which is slightly more than the upper bound limit proposed by Paulay and Priestley [5].

Figure 12b shows the response of the east boundary region in terms of development of out-of-plane deformation at different stages of loading. This boundary region exhibited a similar trend for initiation, increase and recovery of out-of-plane deformation as in the west boundary region. When the specimen was being loaded towards 3.0% drift after unloading from the second -2.5% drift, the out-of-plane displacement reached a normalized value of $\xi = -0.35$, which decreased to $\xi = -0.18$ (2.5% drift cycle) following the initiation of crack closure. However, unlike in the previous cycles and in the west boundary region, the out-of-plane displacement here increased again to $\xi = -0.23$ during 3.0% drift cycle. The concrete crushing was observed at the inner face of the section. Since concrete contributed to the load carrying capacity of the specimen after the crack closure at inner face, leading to recovery of the out-of-plane displacement, this concrete crushing resulted in changing the trend and increasing the out-of-plane deformation. This point corresponds to Point *e* in Figure 2, which was considered as the limit state for calculation of the out-of-plane displacement by Paulay and Priestley [5] and Chai and Elayer [6]. If the specimen had been loaded further in this direction, the concrete crushing would have resulted in steady increase of the out-of-plane deformation and instability of the specimen. Only about half of the residual out-of-plane displacement created in the east boundary region recovered when the specimen was unloaded from 3.0% drift level and was being reloaded in the opposite direction before the global instability of the specimen occurred.

Using Equation 3, the stability criterion proposed by Paulay and Priestley [5] and used by Chai and Elayer [6] has been calculated for the specimen as $\xi_c = 0.15$. This stability criterion is plotted in Figure 12, as well. As shown in this figure, before reaching this criterion, the out-of-plane displacement could be recovered to a great extent. When the maximum out-of-plane displacement exceeded this criterion, relatively considerable residual out-of-plane displacements were created in the boundary regions that would have resulted in instability of the specimen if the loading was continued in the same direction. This residual out-of-plane displacement could have been created due to the initiation of concrete crushing in the concave face of the section exhibiting maximum out-of-plane deformation, which is the limit state used for derivation of the stability criterion.

Paulay and Priestley [5] and Chai and Elayer [6] proposed Equation 1 and Equation 7, respectively, as relationships between the maximum tensile strain ε_{sm} over l_o and the normalized out-of-plane displacement ξ. The plastic hinge length, l_p (given by Equation 8), was postulated to be a reasonable approximation of the potential height of the wall over which out-of-plane buckling may occur, l_o.

$$l_p = 0.2l_w + 0.044h_w \tag{8}$$

where

l_w= horizontal length of the wall section

h_w= full height of the cantilever wall

In order to compare this assumption with the experimental observations, the out-of-plane displacement profile of the west boundary region at the 1.5% (corresponding to initiation of out-of-plane deformation) is plotted in Figure 13a. The plastic hinge length calculated for the specimen using Equation 8 is 584 mm. The corresponding height is denoted in this figure as l_p which is significantly below the height of the out-of-plane displacement profile (visual buckling length of the wall), indicated as l_o (1.5%). The value of l_o does obviously change with the applied lateral drift level as the increase in the applied lateral displacement results in variation of the maximum tensile strain gradient along the height of the boundary regions and consequently also the distribution of the residual crack at the onset of out-of-plane deformation. The maximum tensile strain measurements along the height of the west boundary region during the 1.5% drift cycle and two prior drift cycles (1.0% and 0.75% drift levels) are plotted in Figure 13b and the corresponding average concrete strain profiles calculated using measurements of the linear potentiometers are displayed in Figure 13c. The elevation corresponding to the maximum out-of-plane deformation is denoted as "OOP max".

During the 1.5% drift cycle, the initial out-of-plane deformation was observed in both boundary zones. As can be seen in Figure 13b, during 0.75% and 1.0% drift cycles, plasticity was developed along a distance from the base to 800 mm above. The 0.75% drift level is the stage where overall yielding of the specimen had just taken place. The strain variation at this stage indicates yielding up to the height of about 1100 mm from the base. During the subsequent drift cycle (1.00%), yielding was measured up to the same elevation as the 0.75% drift level. However, the amount of plastic strain developed at the base was considerably larger (about 6 times the yield strain). At 1.5% drift level, the amount of yielding in tension extended up to the height of 1230 mm from the base and the maximum strain at the base was about 10 times the yield strain. When the specimen was unloaded from this stage and was being reloaded in the opposite direction, the out-of-plane deformation started in the west boundary region as shown in Figure 13a. This figure shows that the height of the wall effectively involved in formation of the out-of-plane deformation was about

1200 mm during the 1.5% drift cycle. It should be noted that this out-of-plane displacement profile was measured using 5 potentiometers uniformly spaced along the height of 1230 mm from the base and would not represent the exact displacement pattern, particularly above this elevation. The amount of plastic strain developed in the extreme end reinforcement at the height corresponding to the maximum out-of-plane deformation (600 mm from the base) was slightly bigger than six times the yield strain of the reinforcement. The value of l_p, calculated using Equation 8, marked in Figure 13 was almost 50% of the height of the wall involved in initiation of out-of-plane deformation.

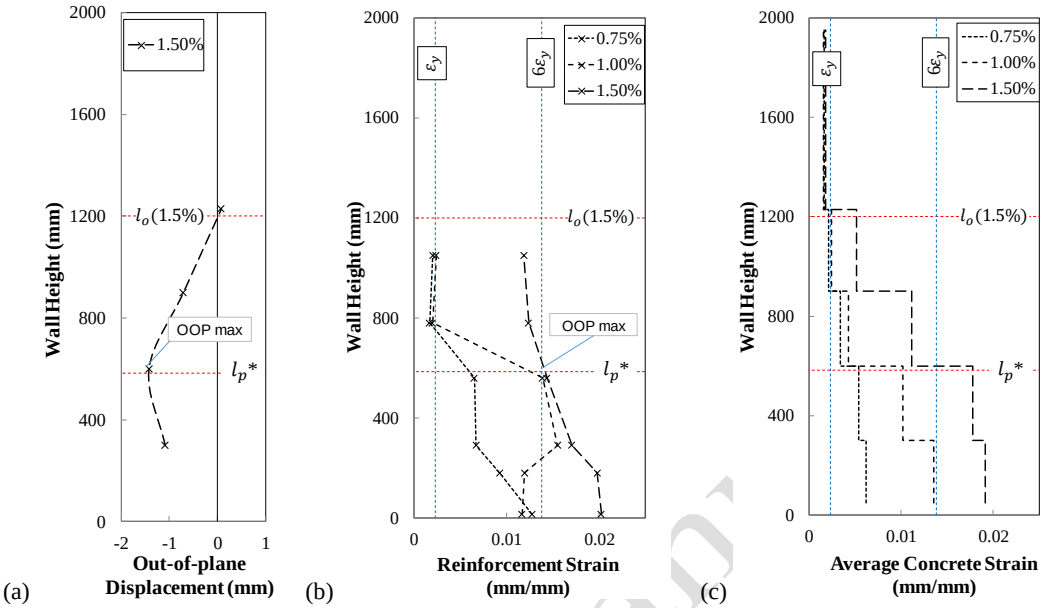

Figure 13. Initiation of out-of-plane displacement at the west boundary: (a) out-of-plane displacement profile; (b) reinforcement strain profiles at peak positive drift levels; (c) average concrete strain profile at peak positive drift levels; * the value of l_p is calculated using Equation 8

Figure 14 displays the evolution of out-of-plane deformation in both boundary regions during all the applied drift cycles starting from the 1.5% drift cycle. The maximum tensile strain measurements within a given loading cycle are also presented in this figure. Since the reinforcement strain gauge measurements were not attainable for the strain values greater than 0.02, due to functionality limit of these gauges, only the average concrete strain measurements within the gauge length of the linear potentiometers, normalized by yield strain are indicated in these figures. The effective height involved in development of out-of-plane deformation (l_o) during the 2.5% drift cycle is also indicated for both boundary regions. This height could not be measured using the out-of-plane displacement measurement at 2.5% and 3.0% drift cycles as this measurement was limited to the elevation of 1230 mm. The values of the buckling height during the 2.5% drift cycle, $l_o = 1430$ (west boundary) and $l_o = 1400$ (east boundary), are therefore corresponding to observation of a wide crack across the thickness that does not follow the same trend as the cracks below this point. This height is approximately two times the height corresponding to the maximum out-of-plane displacement and is about 70% of the wall height. The maximum tensile strain during the 2.5% drift cycle and at the elevation of the maximum out-of-plane deformation is about $7.4\varepsilon_y$ and $7.2\varepsilon_y$ for the west and east boundary regions, respectively.

As noted above, Equation 1 and Equation 7 were proposed by Paulay and Priestley [5] and Chai and Elayer [6], respectively, as relationships between the maximum tensile strain ε_{sm} over l_o and the normalized out-of-plane displacement ξ. Using the experimental measurements of the normalized out-of-plane displacement ξ, the relationship between ε_{sm} and l_o as per these equations and corresponding to the 2.5% drift cycle is plotted in Figure 15. The plots are presented separately for the boundary regions as they exhibited different values of ξ. As also mentioned in Section 2, ε_{sm} corresponds to the strain generating elongation of the vertical reinforcement over the length l_o (i.e., $\Delta l_o = \varepsilon_{sm} l_o$). Considering the measured strain gradients of the specimen within the extent of l_o (shown in Figure 14) the average strain within the extent of the l_o measured in the test is used for comparison of these curves with test measurements. As can be seen in Figure 15, consideration of the plastic hinge length (Equation 8) as the buckling length, l_o, results in a significant overestimation of the maximum tensile strain, ε_{sm}.

However, with the experimentally observed buckling length (about 70% of the unsupported height) both equations provide a relatively good estimation of the maximum tensile strain that could trigger out-of-plane instability of rectangular walls. It is notable that the equation proposed by Chai and Elayer [6] (Equation 3) gives better prediction for this specimen. The main differences between these two approaches are: i) consideration of a sinusoidal curvature

distribution by Chai and Elayer [6] compared to the circular shape idealization of Paulay and Priestley [5] and ii) the maximum tensile strain, ε_{sm}, proposed by Chai and Elayer [6] (Equation 7) includes two more components as the elastic strain recovery, ε_e, and a reloading strain, ε_r, associated with compression yielding of the reinforcement.

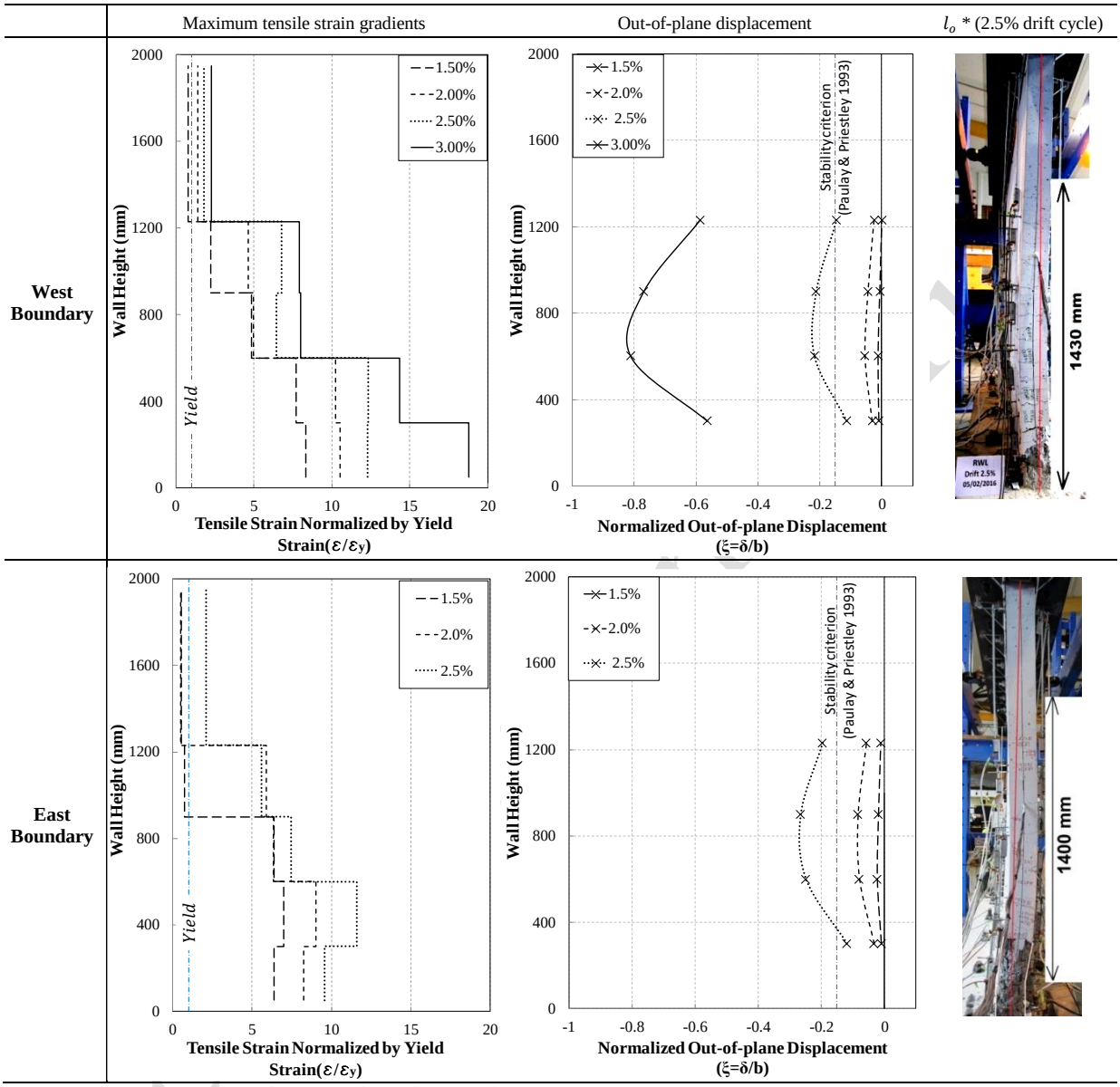

*Height of the wall involved in formation of out-of-plane deformation

Figure 14: Maximum tensile strain and out-of-plane response during different loading cycles

The inconsistency between assumption of $l_o = l_p$ and the experimental measurements of l_o had been observed by Rosso et al. [12] and Johnson [3] as well. The value of l_o was identified as 75% of the wall unsupported height for two singly reinforced wall specimens tested by Rosso et al. [12]. Johnson [3] evaluated the method proposed by Paulay and Priestley [5] with the test data and observed that the critical buckling thickness calculated using this approach was smaller than the thickness of the tested specimens that had exhibited out-of-plane instability. However, more reasonable values were obtained when the height of first yield was considered as the buckling length instead of the length of plastic hinge. The height of the maximum out-of-plane displacement, let alone the entire length of out-of-plane deformation, was more than two times the plastic hinge length calculated using Equation 8. It should be noted that the specimens tested by Johnson [3] were representing walls of a 6-story building and lateral supports were not provided at story levels against out-of-plane deformations. The values of buckling length observed in this study is about 70% of the unsupported height (story level) and is fairly close to the estimation of 75% of the unsupported height proposed by Rosso et al. [12].

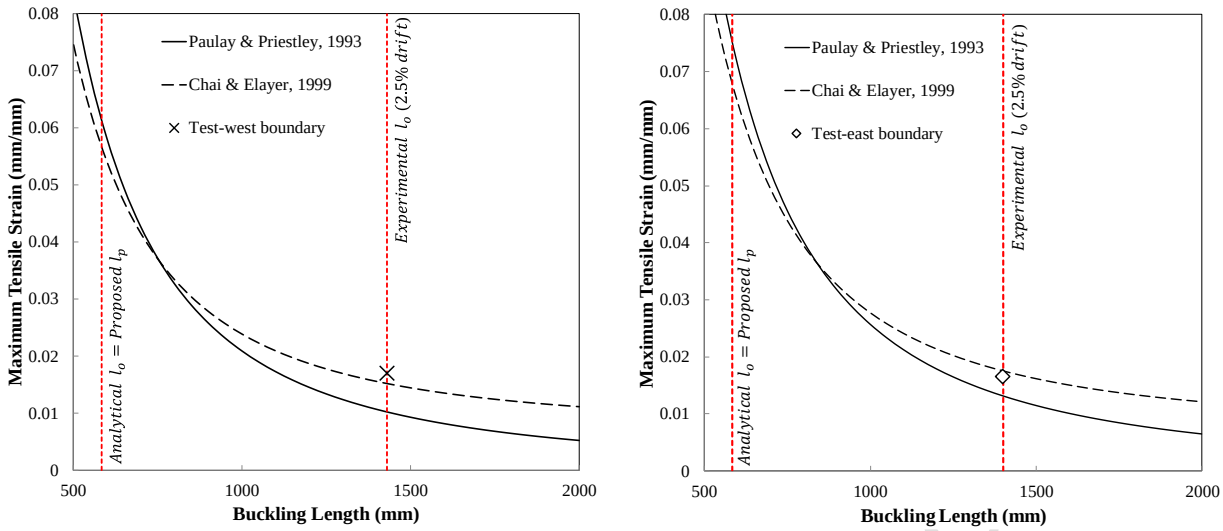

Figure 15. Effect of buckling length on prediction of the maximum tensile strain: (a) west boundary; (b) east boundary

The following stages describe the out-of-plane response of the tested specimen in relation with the previously imposed tensile strain gradients in the boundary regions and the stability criterion proposed in the existing analytical models:

i. Minimal or no out-of-plane deformation

ii. Development of out-of-plane deformation during unloading and reloading stages of a cyclic loading and its rather complete recovery at peak displacement level in the opposite direction, with negligible residual out-of-plane deformation. This stage was associated with an average previously experienced maximum bar strain of about $\varepsilon_{sm} = 0.014$ (about $6\varepsilon_y$ for the tested specimen) within a height equivalent to 60% of the unsupported height of the wall.

iii. Development of out-of-plane deformation during unloading and reloading stages of a cyclic loading and its partial recovery at peak displacement level in the opposite direction, resulting in considerable residual out-of-plane deformation. This stage corresponded to an out-of-plane deformation greater than the stability criterion proposed by the analytical models ($\xi > \xi_c$) and was associated with an average previously experienced maximum bar strain of about $\varepsilon_{sm} = 0.017$(about $7.2\varepsilon_y$ for the tested specimen) within a height equivalent to 70% of the unsupported height of the wall. This height (referred to as l_o) was involved in formation of out-of-plane deformation with the maximum value of out-of-plane deformation occurring roughly at $0.5l_o$. This stage was the limit state for OOP instability as the wall would eventually become unstable if continuously loaded in the same direction and the limits given in literature correspond to this limit.

iv. Development of out-of-plane deformation during unloading and reloading stages of a cyclic loading and its steady increase resulting in out-of-plane instability of the wall. This stage corresponded to an out-of-plane deformation greater than the upper bound limit proposed by the analytical models, i.e., half of the wall thickness ($\xi > 0.5b$) and was associated with an average previously experienced maximum bar strain of about $\varepsilon_{sm} = 0.023$ (about $10\varepsilon_y$ for the tested specimen) within a height equivalent to 70% of the unsupported height of the wall.

The assumptions made in the analytical models regarding the height of the wall effectively involved in formation of out-of-plane deformations (l_o) need to be revised. The test measurements indicate that the out-of-plane deformation profile, i.e., the elevation corresponding to the maximum out-of-plane deformation and the buckling height correlate well with profile of the plastic strain along the height of the wall. The elevation corresponding to the maximum out-of-plane deformation is approximately equal to the plastic hinge length proposed in literature, and the value of l_o is about twice this length.

Based on the experimental results presented in this section, in addition to the value of the previously imposed maximum tensile strain, distribution of this strain along the height of the boundary zones affects development of out-of-plane deformation in rectangular walls. The strain gradients of the tested specimen indicated concentration of tensile strain within a specific height from the base of the specimen. With this strain distribution, compression yielding of the longitudinal bars occurred during unloading and reloading before the cracks closed, which provided ideal circumstances for the inherent eccentricities in construction, material response and loading to cause the boundary region to move in the out-of-plane direction. This height was therefore found to be associated with the buckling length

(l_o) and the maximum out-of-plane displacement was observed at the elevation corresponding to approximately half of this height. Had the strains been localized more at the base region due to phenomena like bond deterioration and premature bar buckling, the yielding in compression would not have occurred along a sufficient height to create a decent out-of-plane displacement profile. These phenomena (i.e., bar fracture and bar buckling) may also interfere with previously initiated progression of out-of-plane deformation and alter the ultimate failure pattern of the wall.

7. EFFECT OF COVER SPALLING AT THE BASE

In literature [20, 21], asymmetric spalling of concrete cover has been postulated to be one of the factors contributing to out-of-plane deformation of rectangular walls under cyclic loading. In this section, the effect of cover spalling on development of out-of-plane deformation is investigated. Figure 16 shows the initiation and development of cover spalling observed in the east and west boundary regions of Specimen RWL and during the 1.5% and 2.0% drift cycles. As can be seen in this figure, although these drift levels (1.5% and 2.0%) correspond to initiation and increase of out-of-plane deformations, the cover concrete had spalled off quite symmetrically at these stages. Also, considering the very limited area of spalled cover concrete compared to the length of boundary regions, its asymmetric spalling would not have a noticeable effect on initiation and development of out-of-plane deformation.

Figure 17 shows the out-of-plane deformation of the wall boundary regions at 2.5% drift cycle. As can be seen in this figure, cover spalling is less likely to affect this phenomenon as the out-of-plane deformations usually start at a considerably higher elevation from the base while cover spalling due to in-plane loading happens at the base region. Moreover, out-of-plane deformation develops when the cracks are wide open (and the compressive forces are taken by the reinforcement only) and reaches its maximum value at around zero displacement of each cycle, whereas cover spalling happens at the peak of the displacement cycles when one of the end regions is under high compression at the base. When the amount of out-of-plane deformation results in crack closure in one face of the wall, the out-of-plane deformation starts to recover as concrete starts to contribute to the load carrying capacity of the wall section. The recovery of out-of-plane deformation prevents the application of considerable compressive stresses to the face of the wall that has experienced this crack closure. Therefore, as cover spalling does not happen at this elevation it cannot affect this mode of deformation. However, at ultimate stages of loading, when the out-of-plane deformation does not fully recover at the peak displacement level, cover spalling may initiate at the elevation where the maximum out-of-plane deformation happens.

Cover spalling at the base occurred symmetrically along the wall thickness. Due to the evolution and recovery trend of the out-of-plane deformation (which becomes maximum at around 0.0% drift during unloading/reloading, when the compression on concrete cover from in-plane loading is minimum), any asymmetric response of concrete would not affect its initiation. The excessive amount of out-of-plane deformation can however result in formation of asymmetric cover spalling at the elevation where the out-of-plane displacement is maximum.

1.5% 2.0% 1.5% 2.0%

(a) West boundary **(b) East boundary**

Figure 16. Cover spalling at the base of the specimen

8. CONCLUSIONS

In order to investigate the causes and evolution of out-of-plane deformation and subsequent out-of-plane instability, the experimental response of a rectangular wall specimen that failed in out-of-plane instability mode under concentric in-plane cyclic loading is dissected in great details in this paper. Out-of-plane instability was the primary failure pattern that was observed in the test, and the wall response was not influenced by other failure patterns such as bar buckling. Therefore, the observations were used to scrutinize the mechanisms leading to out-of-plane instability and the main findings from this study are summarized below:

- The sequence of events observed in the tested specimen were in good agreement with the findings and postulations presented in past research on development of out-plane instability in rectangular walls and concrete columns representing the boundary zones of walls.

- The evolution and recovery of out-of-plane deformation does not cause any strength degradation in the lateral load-top displacement response of the wall. The subsequent possible instability, however, is associated with an instantaneous drop of strength. Therefore, buildings with walls prone to instability failure are likely to undergo large lateral deformations and exhibit progressive collapse as this mode of failure induces a very abrupt loss of lateral load resistance.
- The out-of-plane response of the tested specimen had four stages of: i) minimal or no, ii) fully recoverable, iii) partially recoverable and iv) irrecoverable out-of-plane deformation. These stages were in correlation with the stability criterion and upper bound limits proposed in the existing analytical models.
- In addition to the value of the previously imposed maximum tensile strain, distribution of this strain along the height of the boundary zones also affects the development of out-of-plane deformation in rectangular walls.
- Variation of the induced maximum tensile strain along the wall thickness due to material and loading imperfections could be considered as one of the major sources of inherent eccentricity during unloading and reloading stages.
- The evolution of out-of-plane instability observed in the test was in line with the mechanism simulated by the numerical model previously investigated by the authors.
- The assumptions made in the analytical models and design guidelines regarding the height of the wall effectively involved in formation of out-of-plane deformations need to be revised.
- Cover spalling at the base does not affect evolution of global out-of-plane instability in structural walls.

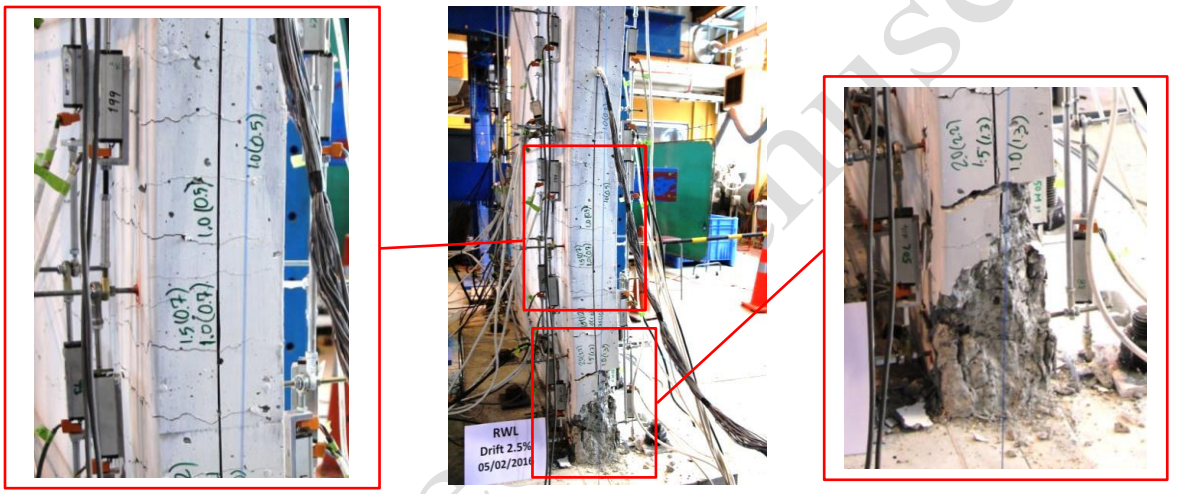

(a) West boundary

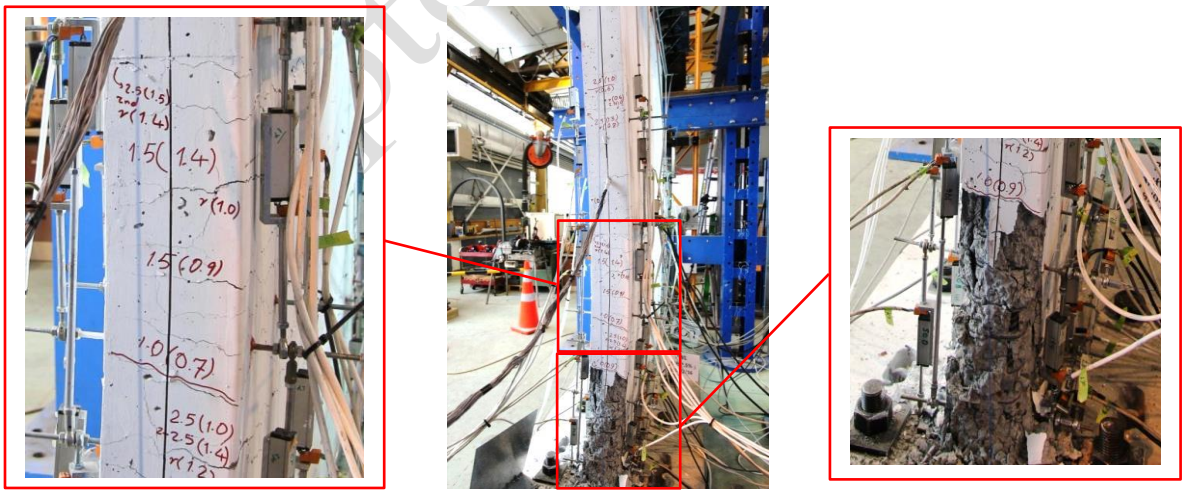

(b) East boundary

Figure 17. Crack pattern and cover spalling corresponding to maximum out-of-plane deformation during 2.5% drift cycle

9. ACKNOWLEDGEMENTS

The authors wish to acknowledge the financial support provided by the Natural Hazard Research Platform (NHRP), the Ministry of Business, Innovation and Employment (MBIE) and the Quake Centre at the University of Canterbury to conduct this research as well as the specimen fabrication scrupulously done by Bradford Precast. The considerate technician support provided by Alan Thirlwell at the University of Canterbury is also greatly appreciated.

10. REFERENCES

1 Sritharan S, Beyer K, Henry R S, Chai Y, Kowalsky M, Bull D. Understanding poor seismic performance of concrete walls and design implications. *Earthquake Spectra* 2014; **30**(1): p. 307-334.
2 Oesterle R, *Earthquake Resistant Structural Walls: Tests of Isolated Walls*. 1976, Research and Development Construction Technology Laboratories, Portland Cement Association.
3 Johnson B, *Anchorage detailing effects on lateral deformation components of R/C shear walls*. 2010, Master Thesis, University of Minnesota.
4 Goodsir W J, *The design of coupled frame-wall structures for seismic actions*. 1985, University of Canterbury.
5 Paulay T, Priestley M. Stability of ductile structural walls. *ACI Structural Journal* 1993; **90**(4): p. 385-392.
6 Chai Y H, Elayer D T. Lateral stability of reinforced concrete columns under axial reversed cyclic tension and compression. *ACI Structural Journal* 1999; **96**(5): p. 780-789.
7 Creagh A, Acevedo C, Moehle J, Hassan W, Tanyeri A C. Seismic performance of concrete special boundary element. *University of Texas at Austin and University of California Berkley, Austin, Berkley* 2010.
8 Chrysanidis T, Tegos I. The influence of tension strain of wall ends to their resistance against lateral instability for low-reinforced concrete walls. *15 WCEE* 2012.
9 Shea M, Wallace J W, Segura C. Seismic performance of thin reinforced concrete shear wall boundaries. 2013.
10 Rosso A, Jiménez-Roa L A, de Almeida J P, Zuniga A P G, Blandón C A, Bonett R L, Beyer K. Cyclic tensile-compressive tests on thin concrete boundary elements with a single layer of reinforcement prone to out-of-plane instability. *Bulletin of Earthquake Engineering* 2017. DOI: 10.1007/s10518-017-0228-1.
11 Haro A G, Kowalsky M, Chai Y H, Lucier G W. Boundary Elements of Special Reinforced Concrete Walls Tested Under Different Loading Paths. *Earthquake Spectra*; **0**(0): p. null. DOI: 10.1193/081617eqs160m.
12 Rosso A, Almeida J, Beyer K. Stability of thin reinforced concrete walls under cyclic loads: state-of-the-art and new experimental findings. *Bulletin of Earthquake Engineering* 2015: p. 1-30. DOI: 10.1007/s10518-015-9827-x.
13 Dashti F, *Out-of-plane Instability of Rectangular Reinforced Concrete Walls Under In-plane Loading*. 2017, PhD Thesis, Department of Civil and Natural Resources Engineering, University of Canterbury. p. 294.
14 Dashti F, Dhakal R P, Pampanin S. Numerical Modeling of Rectangular Reinforced Concrete Structural Walls. *Journal of Structural Engineering* 2017; **143**(6). DOI: 10.1061/(ASCE)ST.1943-541X.0001729.
15 Dashti F, Dhakal R P, Pampanin S. Validation of a Numerical Model for Prediction of Out-of-plane Instability in Ductile Structural Walls under Concentric In-plane Cyclic Loading *Journal of Structural Engineering* 2018b. DOI: 10.1061/(ASCE)ST.1943-541X.0002013.
16 Dashti F, Dhakal R P, Pampanin S. Blind prediction of in-plane and out-of-plane responses for a thin singly reinforced concrete flanged wall specimen. *Bulletin of Earthquake Engineering* 2018a; **16**(1): p. 427–458. DOI: 10.1007/s10518-017-0211-x.
17 Dashti F, Dhakal R, Pampanin S. *Development of out-of-plane instability in rectangular RC structural walls* in *2015 NZSEE Conference*. 2015. Rotorua, New Zealand: New Zealand Society for Earthquake Engineering.
18 Dashti F, Dhakal R P, Pampanin S, *Simulation of out-of-plane instability in rectangular RC structural walls*, in *Second European Conference on Earthquake Engineering and Seismology*. 2014: Istanbul, Turkey.
19 Dashti F, Dhakal R P, Pampanin S. Tests on slender ductile structural walls designed according to New Zealand standard *Bulletin of the New Zealand Society for Earthquake Engineering* 2017; **50**(4): p. 504-516.
20 Vallenas J M, Bertero V V, Popov E P, *Hysteretic behaviour of reinforced concrete structural walls*, in *Report no. UCB/EERC-79/20*. 1979, Earthquake Engineering Research Center, University of California, Berkeley.
21 Hilson C, Segura C, Wallace J, *Experimental study of longitudinal reinforcement buckling in reinforced concrete structural wall boundary elements*, in *Tenth U.S. National Conference on Earthquake Engineering (10NCEE)*. 2014: Anchorage, Alaska.

The final publication is available at Earthquake Engng Struct Dyn. 2018;1–21. https://doi.org/10.1002/eqe.3115

Table 1. Behavior of wall end-region under the loading cycle shown in Figure 2

	Path	
Loading	*o-a*	Large tensile strain
Unloading	*a-b*	Elastic strain recovery mainly in reinforcing steel
Reloading	*b-c*	Reloading in compression on the cracked concrete column accompanied by an out-of-plane displacement; yielding of the reinforcement closer to the applied axial force resulting in a reduced transverse stiffness of the column and an increased out-of-plane displacement.
	c-d	Compression yielding in the second layer of the reinforcement, and a rapid increase in the out-of-plane displacement
	d-e	Closure of cracks at Point d and decrease of out-of-plane displacement and increase of out-of-plane displacement after significant compressive strain is developed in the compressed concrete
	d-f	An excessive crack opening where subsequent compression would not result in the closure of the cracks but a continued increase in the out-of-plane displacement and eventual buckling of the column